buildings

MDPI

Article

Experimental Study on the Mechanical Properties of Reinforced Pervious Concrete

Ming-Gin Lee [1,*], Yung-Chih Wang [2], Wei-Chien Wang [2], Hung-Jen Chien [2] and Li-Chi Cheng [1]

[1] Department of Construction Engineering, Chaoyang University of Technology, Taichung 413, Taiwan; a0979266737@gmail.com
[2] Department of Civil Engineering, National Central University, Taoyuan 320, Taiwan; wangyc@ncu.edu.tw (Y.-C.W.); a654.joy@gmail.com (W.-C.W.); joe86010910@yahoo.com.tw (H.-J.C.)
* Correspondence: mglee@cyut.edu.tw

Abstract: Pervious concrete (PC) has gained popularity as an environmentally friendly solution for mitigating the urban heat island effect and promoting sustainable construction. However, its lower compressive strength, attributed to its higher porosity required for permeability, poses challenges for withstanding heavy vehicle loads on pavements. Our study aims to improve the flexural strength of regular PC by adding advanced reinforcing materials like steel wire mesh or glass fiber mesh. This results in reinforced pervious concrete, referred to as RPC, which offers enhanced strength and durability. The primary objective of our research is to investigate the mechanical behavior of RPC, with a specific emphasis on essential design parameters such as PC elastic modulus, modulus of rupture, and stress–strain characteristics under both single and repeated loading conditions. Our findings reveal that the influence of repeated loading on the compressive strength and elastic modulus of PC pavement is negligible, as there are no significant differences observed between the two loading protocols. Notably, our statistical analysis indicates that the PC strength (fc′) averages around 15 MPa. Moreover, empirical formulas for the elastic modulus (Ec = $3072\sqrt{f_c{}'}$) and modulus of rupture (fr = $0.86\sqrt{f_c{}'}$) are derived from our research. Furthermore, our study establishes that the stress–strain behavior of PC closely aligns with the general concrete model proposed by a previous scholar, providing valuable insights into the material's structural performance. These findings contribute to a better understanding of RPC's mechanical properties and offer potential solutions for improving its suitability for heavier vehicular loads.

Keywords: green building material; reinforced pervious concrete; glass fiber mesh; steel wire mesh; elastic modulus; modulus of rupture

check for updates

Citation: Lee, M.-G.; Wang, Y.-C.; Wang, W.-C.; Chien, H.-J.; Cheng, L.-C. Experimental Study on the Mechanical Properties of Reinforced Pervious Concrete. *Buildings* **2023**, *13*, 2880. https://doi.org/10.3390/buildings13112880

Academic Editor: Antonio Caggiano

Received: 12 October 2023
Revised: 11 November 2023
Accepted: 15 November 2023
Published: 17 November 2023

Copyright: © 2023 by the authors. Licensee MDPI, Basel, Switzerland. This article is an open access article distributed under the terms and conditions of the Creative Commons Attribution (CC BY) license (https://creativecommons.org/licenses/by/4.0/).

1. Introduction

Traditional asphalt concrete pavement is prone to the heat island effect. Due to the dark color of the pavement, the albedo is low. During the day, the pavement absorbs a large amount of high temperature and solar radiation, making the pavement temperature higher than the atmospheric temperature and unable to release energy until the atmospheric temperature drops at night. This phenomenon results in higher temperatures in urban areas during both day and night compared to suburban areas. To mitigate the occurrence of the heat island effect, it is generally recommended to install porous pavements. These pavements enhance the flow of heat energy between the atmosphere and the soil. Additionally, the color of porous concrete, resembling gray, contributes to increased albedo and lower heat absorption capacity, thereby diminishing the accumulation of heat energy in the pavement [1,2].

The surface temperature of porous pavement can also drop rapidly in the evening, which can effectively reduce the formation of the heat island effect in urban areas. Therefore, pervious concrete serves as the central theme of this study. The literature review primarily concentrates on research papers related to the mechanical behavior of pervious concrete pavement, encompassing topics such as pervious concrete proportions, reinforcing mesh materials, and mechanical behavior patterns regarding concrete compression and deflection, among others [3–5].

The main method of reinforcing concrete is to add scattered fibers or grid-like reinforcements. Fiber concrete (FRC) refers to fibers randomly distributed in concrete to provide tensile strength to achieve a stiffening effect. There are many different types of fibers available for engineering applications today, with choices ranging from synthetic organic materials (such as polypropylene or carbon fibers), to synthetic inorganic materials (such as steel fibers), to natural organics (such as cellulose or sisal) and to naturally occurring inorganic materials (asbestos, etc.). The selection of fibers depends on the properties of the fibers, such as diameter, specific gravity, Young's modulus, tensile strength, etc., and the impact of different fibers on the basic properties of cement. In FRC, thousands of fiber filaments are randomly distributed in the concrete through the mixing process. Improving the properties of the concrete in all directions helps to improve the ductility, dry shrinkage cracks, flexural strength and compressive strength. Contains polypropylene fiber concrete has better toughness than fiber-free concrete; adding fiber can prevent surface cracks and improve the tensile strength of concrete [6–9]. However, there are also some problems with loose fibers. For example, glass fibers are soft and easy to deform. During the mixing process, they bond with the cement slurry to form balls or flakes. After hardening, they fail to disperse evenly, causing the affected particles to form. Weak surfaces are formed when pressed, resulting in the phenomenon that the strength of a glass fiber containing less glass fiber is higher than that of a glass fiber containing a large amount of fiber. Therefore, if you need to use loose fibers, you need to start to improve this problem [10–12].

Grid-like reinforcing materials also include glass fiber mesh, steel wire mesh, geofabricated fiber mesh, etc., and related research [13,14] has proven that geofabricated fiber mesh (grade fiber grid) can be used as reinforcing material in permeable concrete. feasibility. Geotextile fiber mesh can further increase the drainage performance design of permeable concrete pavement (porosity > 20%, permeability coefficient > 4.5 mm/s), and has good load-bearing capacity, flexural strength up to 5 MPa, and compressive strength up to 30 MPa. It is worth noting that experimental results show that the best pavement bending strength is obtained when the artificial fiber mesh is placed at both one-third and two-thirds depth. It is also proposed that the load change of the vertical displacement of the geofiber grid beam can be divided into five stages, i.e., a linear elasticity stage, a brittle failure stage, a bearing capacity recovery stage, a bearing capacity loss stage and a residual strength stage [15,16].

Unlike steel that rusts in water, geogrids have good corrosion resistance. Geogrids provide different performances depending on their characteristics such as constituent materials, grid shape, size, location, and number of layers [16,17]. Embedding geogrids in permeable concrete can enhance resistance to reflective cracks (inhibition of reflection cracks) by providing additional tensile strength and ductility [18,19].

Numerous studies on pervious concrete's mechanical properties have been conducted in the past. For instance, Arissaman and colleagues [20] investigated the use of sack fibers (SF) to reinforce recycled aggregate porous concrete, with a focus on enhancing its flexural strength and durability. Sakib and his team [21] reviewed the evolution of sulfur's utilization as a road construction material, emphasizing its applications and technological advancements in pavement construction. Amin and collaborators [22] conducted a study comparing the effectiveness of machine learning methods with traditional ones in predicting the compressive strength of rice husk ash concrete, providing an insightful comparison. Khan et al. [23] showcased the performance of fiber concrete made from recycled aggregates and waste lathe fibers, highlighting its sustainable applications. Karalar et al. [24] introduced the use of dispersed coconut fiber to reinforce normal weight concrete, emphasizing improvements in its stress–strain characteristics. Çelik and colleagues [25] examined the properties of fiber concrete produced with waste lathe fibers, underlining its sustainable applications. Shcherban and his team [26] investigated normal-weight concrete reinforced with dispersed coconut fibers and pointed out enhancements in its stress–strain properties. Zeybek and colleagues [27] explored the properties of fiber concrete made from steel fibers extracted from waste tires, offering an intriguing approach to material recovery and reuse. Finally, Beskopylny and collaborators [28] delved into the impact of using rubber tree seed shell additives on concrete properties, emphasizing the use of sustainable construction materials and recycled resources.

There has been limited research on reinforcing the mechanical properties of pervious concrete pavement. Typically, pervious concrete lacks steel reinforcement, which leaves the bottom layer of the concrete less capable of withstanding tensile forces that occur during cracking. Therefore, the objective of this study is to enhance the mechanical behavior of pervious concrete by incorporating reinforcing materials into the lower layer. This involves the addition of fiberglass mesh and steel wire mesh to the lower layer of pervious concrete, and the study examines the resulting improvements in flexural strength and toughness (referenced in sources [29–33]). In addition, carbon nanotubes [34] are also one of the methods to enhance the structural and mechanical properties of cement-based composites. The above research has the potential to enhance the guidance for reinforced pervious concrete pavement design.

2. Materials and Methods

The commonly used elastic modulus formulas, cracking modulus formulas and concrete stress and strain models are all used to study ordinary normal-weight concrete. This study hopes to use experiments and data statistics to find the elastic modulus and cracking modulus formulas suitable for pervious concrete. The concrete stress–strain curve proposed by Popovics [11] was used as a benchmark for discussion, and the single and repeated compression test results of a Φ100 × 200 mm cylindrical specimen were used for analysis and comparison. The purpose of the repetition is to simulate the repeated driving of a vehicle on the road. Observe the differences before and after iteration for subsequent design use. The materials and methods in this study are described below. The research flowchart of reinforced pervious concrete pavement is shown in Figure 1.

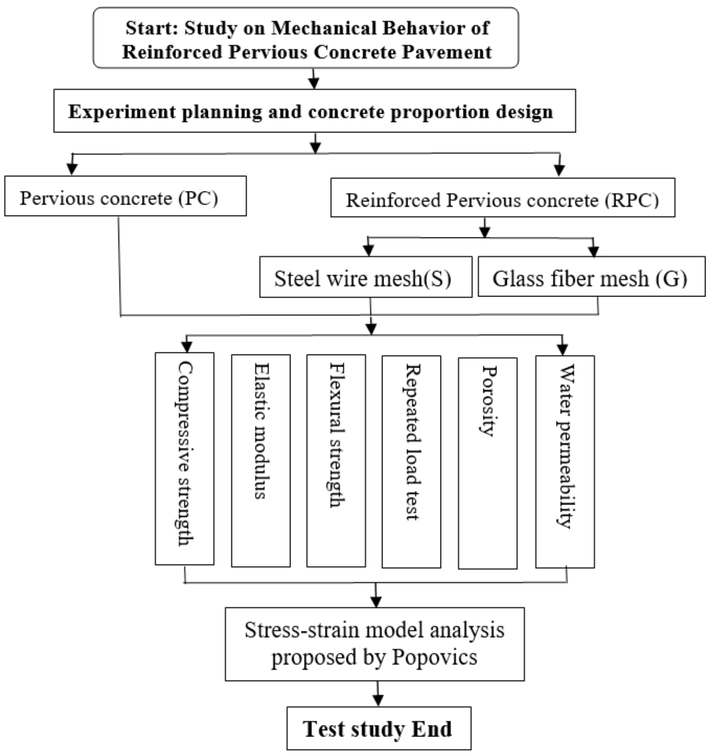

Figure 1. Research flowchart of reinforced pervious concrete pavement.

2.1. Raw Material

The cement used in PC and RPC in this study is Portland Type II cement produced by a local cement company. Portland type II cement is also known as "modified cement". Due to its special properties, it is mostly used to resist moderate sulfate corrosion or massive concrete structures. Its ingredients include tricalcium aluminate (C_3A) content of 5.78%, tricalcium silicate (C_3S) content of 62.00%, dicalcium silicate (C_2S) content of 10.80% and tetracalcium aluminum ferrite (C_4AF) content of 8.70%.

The coarse aggregate used in this study's pervious concrete was excavated from the basement and then crushed, with particle sizes ranging from 9.5 to 4.75 mm. Table 1 displays the gradation and sieve analysis of the coarse aggregate. No fine aggregate was utilized. The superplasticizer was added at a rate of 0.65% by weight of cement. The water-cement ratio (W/C) stood at 0.389, while the aggregate-cement ratio (A/C) was 4.5. The pervious concrete mix design consisted of 340 kg/m^3 of cement, 1530 kg/m^3 of coarse aggregate, 130 kg/m^3 of water, and 2.2 kg/m^3 of superplasticizer.

Table 1. Coarse aggregate gradation and sieve analysis.

Sieve Size	Individual Fraction Retained by Mass (%)	Passing by Mass (%)	Cumulative Retained by Mass (%)
9.5 mm	0	100	0
#4 (4.75 mm)	72.3	27.7	72.3
#8 (2.36 mm)	22.5	5.2	94.8
#16	2.0	3.2	96.8
#30	1.2	2.0	98.0
#50	2.0	0	100
#100	0	0	100
Pan	0	0	100
Fineness modulus = 5.62			

The reinforcing materials used in this study are steel wire mesh and glass fiber mesh. The steel wire is a ϕ5 mm steel wire sold by a built-in wire mesh. The glass fiber mesh is alkali-resistant glass fiber reinforced mesh with low conductivity and an alkali-resistant coating, which complies with EU certification. It is characterized by high tensile strength, low elongation and high temperature resistance. It is available in three specifications: R108, G96 and G120. Its properties are shown in Table 2.

Table 2. Glass fiber mesh specification.

Grid Type	R108	G96	G120
Grid size (mm)	9 × 9	25 × 25	40 × 40
Grid weight (g/m^2)	140	130	145
Chemical coating		Alkali resistant	

2.2. Test Specimens and Methods

The pervious concrete pavement test is mainly divided into two parts: PC and RPC. The RPC part is reinforced with steel wire mesh or glass fiber mesh. The pervious concrete specimen was made as a Φ100 × 200 mm cylindrical specimen, and the compressive strength, elastic modulus, water permeability, and porosity were measured. A rectangular beam specimen of $100^b \times 80^h \times 500^L$mm was used to conduct a bending and deflection test. After the deformation gauge was installed on the beam specimen, it was placed in a universal testing machine for repeated loading. For the flexural strength test, the rectangular beam specimen has Pi gauges attached to both sides 5 mm downward from the top and 5 mm upward from the bottom, as shown in Figure 2. The displacement gauge is a 50 mm Pi-type displacement gauge (PI-5-50) manufactured by an electromechanical company in Tokyo, which is installed above and below the midpoint of both sides of the beam specimen to measure the cracking displacement of the specimen. The method of calculating the strain of pervious concrete is shown in Figure 3. The cylindrical and rectangular beam specimen molds are shown in Figure 4.

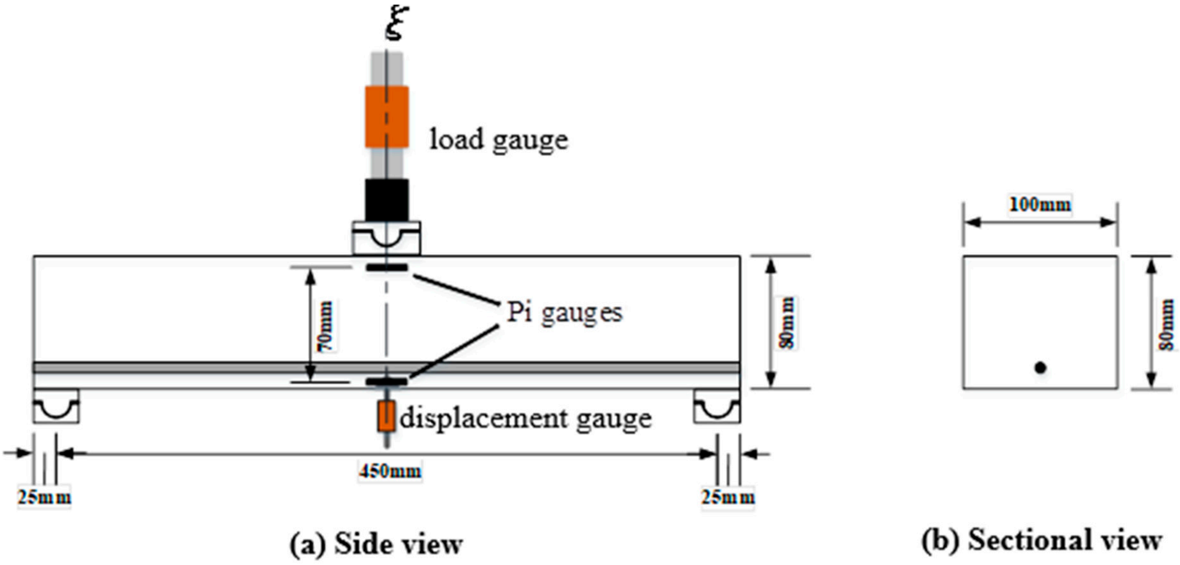

Figure 2. Beam specimen and flexural strength test setup.

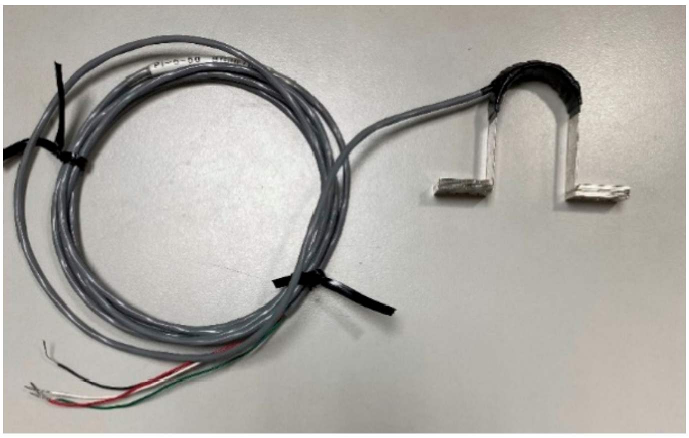

Figure 3. Pi-type displacement gauge (PI-5-50).

(**a**) (**b**)

Figure 4. Specimen molds: (**a**) cylindrical specimen mold and (**b**) beam specimen mold.

The specimen codes in this study are arranged in the following order: strength, shape, reinforced material, and number of groups (including the number of repeated loads). The strength of the specimen is N (ordinary strength), the cylindrical specimen is C, and the beam specimen is B. If no reinforcing material is added to the specimen, it is O. If there is fiberglass mesh or steel wire mesh, they are represented by G and S, respectively. Cylindrical specimens are numbered from A to C (groups of three), and beam specimens are numbered from 1 to 4. Single loads and 10,000 times and 50,000 times repeated loads are represented by 0, 1 and 5, respectively. Example of sample coding: a cylindrical specimen that has been repeated 10,000 times, which is coded NC-OB(1); the third glass fiber mesh beam specimen with a specimen number of NB-G3.

2.2.1. Compressive Strength Test

Pervious concrete has large pores, and the top and bottom must be covered with gypsum to ensure that the load can be evenly applied to the cylindrical specimen. A universal material testing machine was used to perform a compression test after the specimen was cured for 28 days. The test is controlled by load, and the loading rate was conducted in accordance with the ASTM C39/C39M-16 [35].

2.2.2. Flexural Strength Test

The test was conducted in accordance with the ASTM C78/C78M-18 [36] three-point load bending test specification. After the test, the flexural strength of the beam was calculated using Equation (1).

$$\mathrm{R} = \frac{PL}{bd^2} \tag{1}$$

In the formula, R is the bending failure load (N), P is the maximum load (N), L is the span between supporting rods (mm), b is the width of sample (mm), and d is the depth of sample (mm).

A displacement gauge was erected at both ends of the three-point load bending test specimen to measure the maximum average displacement of the midpoint of the beam, as shown in Figure 5a.

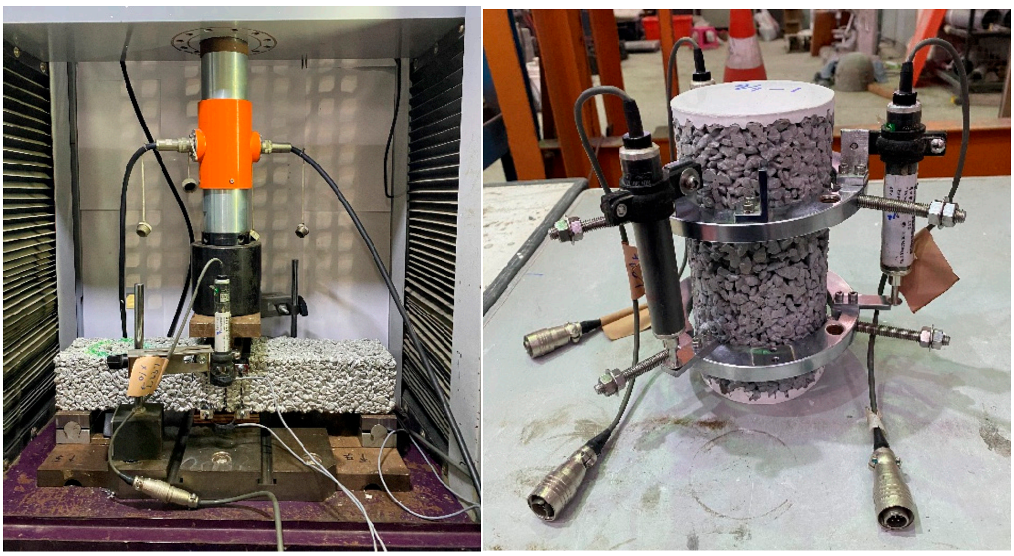

(**a**) Three-point flexural test (**b**) Strain ring and three sets of LVDT installation

Figure 5. Test setup for (**a**) flexural test and (**b**) elastic modulus test.

2.2.3. Elastic Modulus Test

This study refers to the design of the strain ring according to ASTM C469/C469M-22 [37]. The setting is as shown in Figure 5b and the compression test is carried out with the static data capture. After measurement, the data files are simultaneously recorded and stored by the static data retriever, and the elastic modulus of concrete can be calculated using the ASTM C469 formula.

2.2.4. Measurement of Water Permeability Coefficient

The water permeability coefficient k (cm/s) is measured by the Falling-head Test mentioned in ACI 522R-10 [38]. It is derived from soil mechanics and is used in low-permeability soil (k < 10^{-2} cm/s) and refers to the test instrument measured in the literature of Hong et al. [39]. The inner diameter of the upper end of the water pipe is a 95 mm acrylic pipe and is connected to a pervious concrete PVC pipe. The pipes are connected with rubber sleeves and iron rings are used to pressurize them to prevent leakage. The permeability coefficient Equation (2) is as follows:

$$k = \frac{A_1}{A_2} \times \frac{L}{t} \times \ln\left(\frac{h_1}{h_2}\right) \quad (2)$$

In the formula, k is the permeability coefficient (cm/s), A_1 is the cross-sectional area of the upper acrylic tube (cm^2), A_2 is the measure of the cross-sectional area of the test object (cm^2), h1 is the initial water head height (cm), h_2 is the final water head position (cm), L is the height of specimen (cm), and t is the the time it takes for water to flow from h_1 to h_2 (s).

2.2.5. Porosity Measurement Test

The main principle of porosity is the drainage volume method. The porosity is measured according to the test method [40] stipulated in the draft porous concrete performance test method proposed by the Japan Concrete Association in 1998. First, the specimen is immersed in a constant temperature water tank for 24 h, and then its surface is weighed. The dry saturated weight is then placed in the oven at 110 °C for 24 h. Then the weight in water is weighed. Finally, the connected porosity (P_1) is calculated, as shown in Equation (3).

$$P_1 = \frac{1 - (W_1 - W_2)}{V_1} \times 100\% \quad (3)$$

In the formula, P_1 is the connected porosity (%), W_1 is the specimen immersed in water and weighed after being saturated with water, W_2 is the dry internally saturated weight of the specimen soaked in water for 24 h, and V_1 is the volume of the specimen measured and calculated with a caliper.

2.2.6. Repeated Load Test

The compressive repeated-load plan of the cylindrical specimen is shown in Figure 6a. After the strain ring and displacement gauge are installed on the specimen, it is placed in a universal testing machine for repeated-load testing. The repeated-load intensity is 0.5 fc′. When it reaches 10,000 or after 50,000 repetitions, a single pressure failure test was performed, and the fc′ and Ec values were measured at the same time.

The bending repeated-load plan of the beam specimen is shown in Figure 6b. After the deflection gauge is installed on the beam specimen, it is placed in the universal testing machine for repeated-load testing. The repeated-load intensity is 0.6 times the single pressure cracking strength of the beam (Pcr). The data will be recorded every 10,000 cycles to compare the differences. The single pressure failure test will not be conducted until 50,000 cycles.

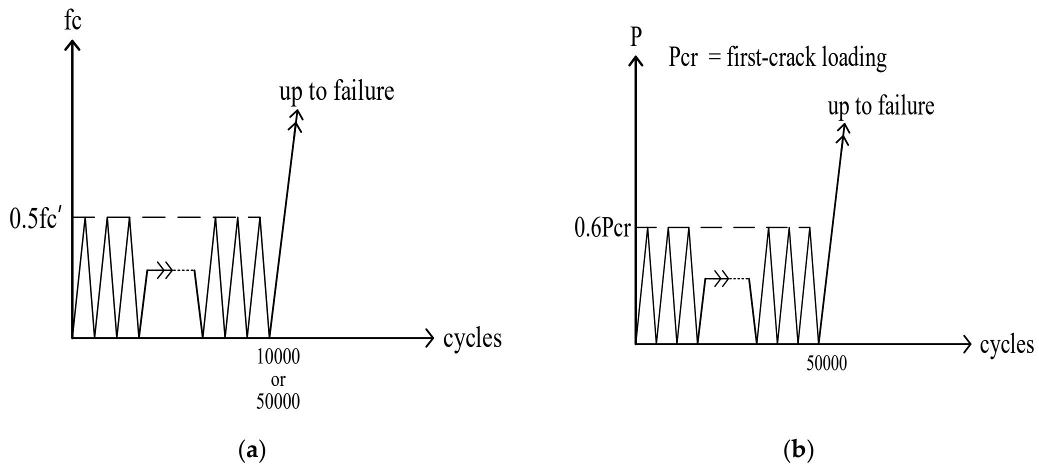

Figure 6. Repeated load test plan (**a**) compressive cylindrical specimen and (**b**) bending beam specimen.

3. Results and Discussion

The test results and discussion of this study encompass material tests on pervious concrete and reinforcing materials, specifically with steel wire mesh or a glass fiber mesh. Additionally, the study covers the stress–strain curve of pervious concrete, the stress–strain curve model, and the mechanical behavior of beams under repeated loading and single-load conditions.

3.1. Results of Material Testing of Pervious Concrete and Reinforcing Material

The basic quality test of pervious concrete in this study involves the permeability coefficient and porosity, with three and six specimens, respectively. Table 3 presents the measurement results for the permeability coefficient and porosity. The study concludes that the permeability coefficient for this pervious concrete is 2.39 cm/s, and the porosity is 20.35%, meeting the requirements outlined in ACI 522R-10 [38].

Table 3. Pervious concrete of water permeability coefficient and porosity.

Pervious Concrete	Mean	Standard Deviation	Coefficient of Variation (%)	ACI 522R-10 Standard
Water permeability coefficient (cm/s)	2.39	0.20	8.17	≥0.1
Porosity (%)	20.35	1.82	8.96	18~35

The reinforcement materials employed in this study included steel mesh and fiberglass mesh. The experimental results for the tensile strength and elastic modulus of single-strand stiffeners from three types of glass fiber mesh and steel wire mesh are presented in Table 4. Corresponding stress–strain curves are depicted in Figure 7.

Table 4. Tensile strength and elastic modulus of glass fiber mesh and steel wire mesh.

Mesh	Code	Width	Diameter/ Thickness (mm)	A_S * (mm^2)	f_u * (MPa)	Δ * (%)	E_C (MPa)
Glass fiber	R108	0.39	0.91	0.35	764	2.26	33,825
	G96	0.51	1.99	1.02	627	1.82	34,461
	G120	0.61	3.26	1.98	655	1.87	35,059
Steel wire	D5	-	5	19.63	621	15	200,000

* Codes (A_S: cross-sectional area, f_u: tensile breaking strength, Δ: elongation).

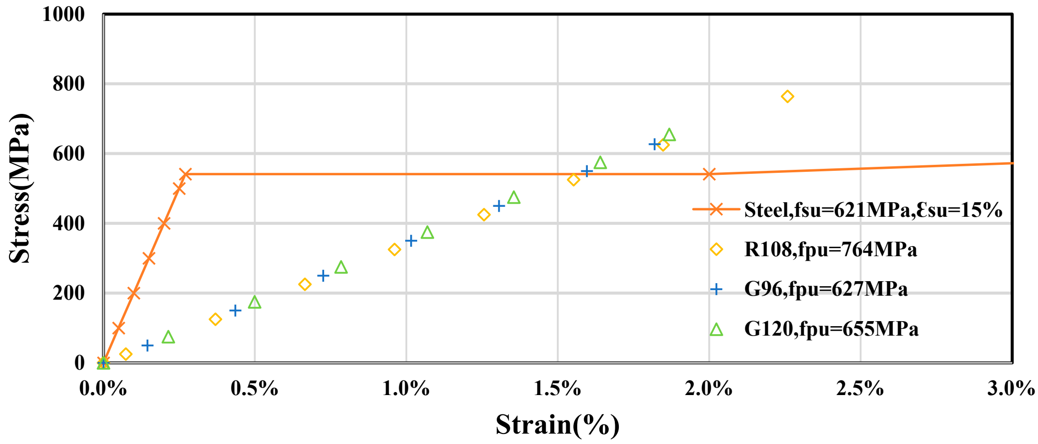

Figure 7. Stress–strain curves of glass fiber mesh and steel wire mesh.

The findings indicate that R108 exhibits the highest tensile strength among the three types of glass fiber mesh, while there is minimal difference in elastic modulus among them. Due to the small grid spacing of R108 (9 × 9 mm), chosen to prevent hindrance to the passage of pervious concrete coarse particles, and its proximity to the tensile strength of steel wire mesh, G96 was selected as the glass fiber mesh reinforcement material in this study.

3.2. Repeated Load Test Results of Pervious Concrete Cylindrical Specimen

After curing the pervious concrete cylindrical specimens for 28 days, both single-load and repeated-load tests were conducted. The repeated-load intensity was controlled at 0.5 times (0.5 fc′) the failure strength of the single load. When the number of repeated loading cycles reaches 10,000 or 50,000 times, a single-pressure failure is performed, and the elastic modulus is measured. The results of both the single-load and repeated-load tests for pervious concrete cylindrical specimens are presented in terms of compressive strength and elastic modulus corresponding to the number of loads, as illustrated in Figure 8. With an increase in the number of repeated loading cycles, both the compressive strength and elastic modulus show a slight increase. This phenomenon is speculated to be related to the porosity size. After repeated loading, the pervious concrete specimen not only avoided damage but also exhibited an effect similar to compacting the pervious concrete, leading to a reduction in porosity size and, consequently, an increase in compressive strength and elastic modulus [2].

When discussing the empirical formula for the elastic modulus of pervious concrete, Lee et al. [7] were included for comparison between ordinary strength and high-strength pervious concrete specimens, as shown in Figure 9. The results indicated a lower average coefficient of elastic modulus. This disparity is likely attributed to the lower compressive strength of pervious concrete compared to ordinary concrete and its relatively larger porosity, resulting in a smaller elastic modulus value. Consequently, this study adopts Equation (4) as the subsequent design calculation of the elastic modulus (E_c) of pervious concrete.

$$E_c = 3072\sqrt{f_c{}'} \quad (4)$$

3.3. Results of Stress and Strain Model of Pervious Concrete

The concrete stress–strain model is generally normal-weight concrete. However, this section studies the stress–strain model of pervious concrete and utilizes the concrete stress–strain curve proposed by Popovics [11] as a reference point for discussion. Both single and repeated compression tests were analysed using Φ100 × 200 mm concrete specimens.

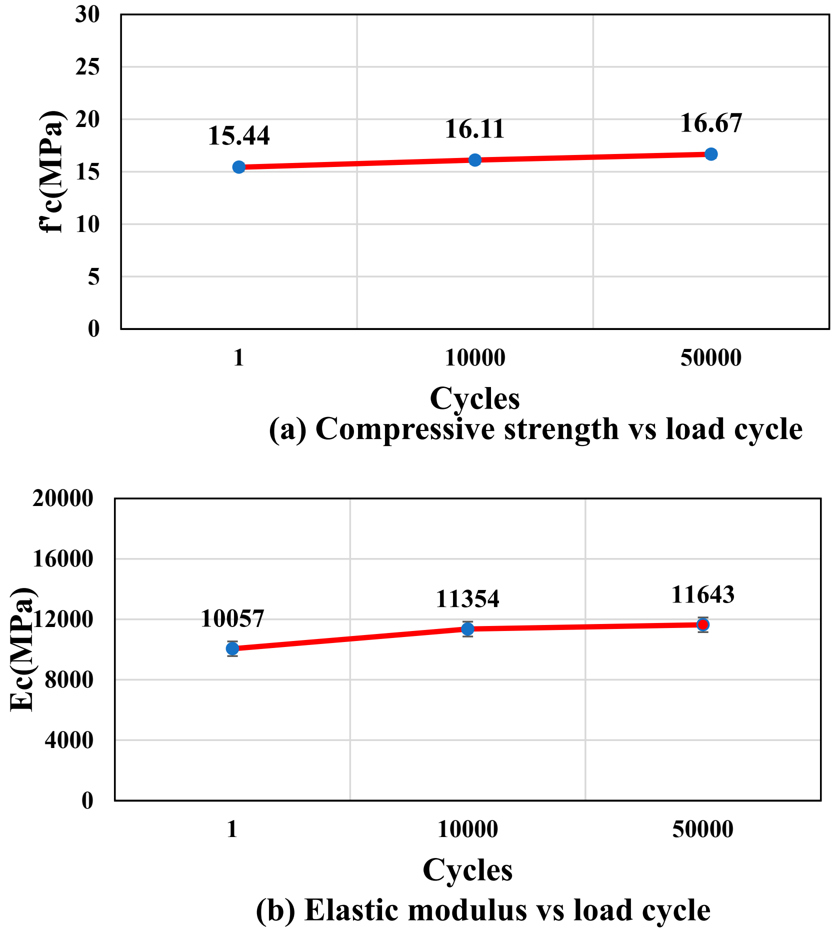

Figure 8. Repeated load test: (**a**) compressive strength and (**b**) elastic modulus of pervious concrete corresponding to load cycles.

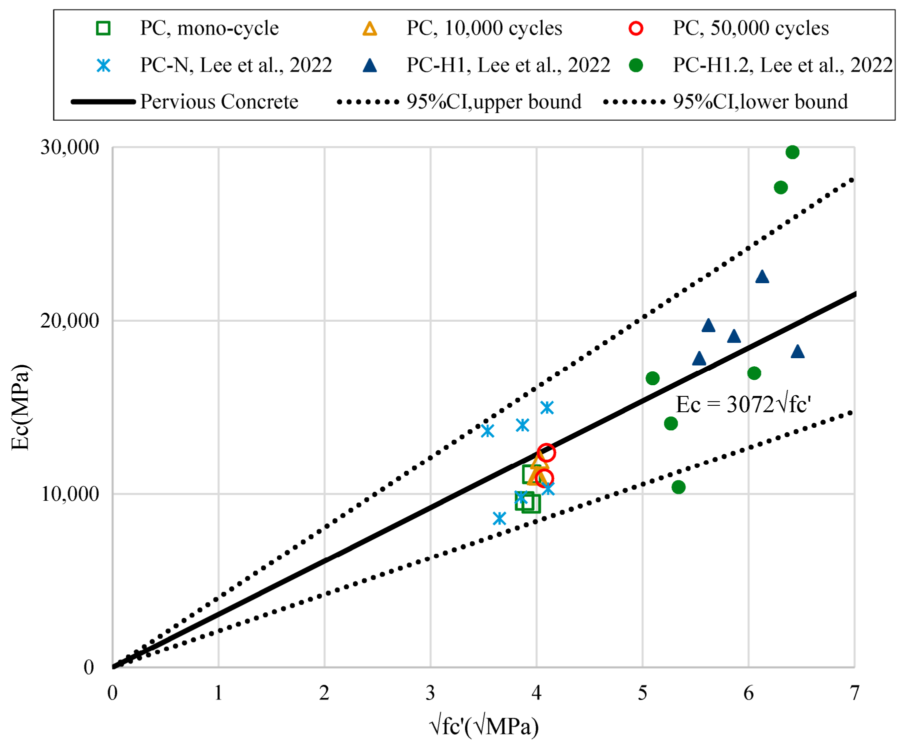

Figure 9. Pervious concrete elastic modulus distribution chart.

3.3.1. Single Compressive Stress–Strain Curve

This study incorporates experimental data from three specimens. Additionally, six specimens with consistent granular materials, permeability coefficients, and porosity, as reported in the study by Lee et al. [7], were selected for a comparative analysis to enhance the credibility of the study. The data are organized in Table 5.

Table 5. Pervious concrete data sheet ($f_c{}'$, $\varepsilon_c{}'$ and E_c).

Specimen#	f_c' (MPa)	ε_c'	E_c (MPa)
NC-O1(0)-1	15.59	0.0019	9438
NC-O1(0)-2	15.62	0.0020	11,125
NC-O1(0)-3	15.10	0.0024	9608
N-O-1 [7]	13.32	0.0018	8605
N-O-2 [7]	12.51	0.0012	13,650
N-O-3 [7]	16.79	0.0017	14,985
N-O-4 [7]	14.95	0.0013	13,984
N-O-5 [7]	16.87	0.0021	10,306
N-O-6 [7]	14.83	0.0031	9816
Mean	15.06	0.002	11,280
Standard deviation	1.43	0.0006	2322
CV (%)	9.5	29.4	20.6

The general formula developed by Popovics [11] examines the axial deformation and formulates a stress–strain model, which is presently a widely adopted theory for simulating reinforced concrete structures. Moehle [9] compiled Popovics' theory and presented the stress–strain relationship curve under various concrete strengths, as depicted in Equation (5).

$$\frac{f_c}{f_c'} = \frac{\varepsilon_c}{\varepsilon_c'} \frac{n}{n - 1 + (\varepsilon_c/\varepsilon_c')^{nk}} \tag{5}$$

In the formula, $f_c{}'$ is the ultimate peak stress of the cylindrical specimen, $\varepsilon_c{}'$ is the strain value when the compressive strength reaches the ultimate peak stress, *n is the* curve fitting factor= $\frac{E_c}{(E_c - E_c')}$, where $E_c' = \frac{f_c'}{\varepsilon_c'}$, and k is the decay factor $k = 0.67 + \frac{f_c'}{62}$(MPa).

According to the concrete stress–strain model formula mentioned above, the average curve parameters can be obtained, as shown in Table 6. Among them, $f_c{}'$, $\varepsilon_c{}'$ and E_c are the average values of the experimental data of each ratio, and $E_c{}'$, n and k are obtained from the empirical formula. The stress–strain curve obtained by bringing the above parameters into Popovics Equation (5) is the red curve in Figure 10 and is compared with other experimental values. It is evident that the experimental values closely resemble the Popovics parameter curve. Therefore, it can be inferred that the stress–strain curve of pervious concrete can also be predicted directly using Equation (5) proposed by Popovics.

Table 6. Stress–strain curve parameters obtained from suggested Equation (5).

Parameter	fc′ (MPa)	εc′ (%)	Ec′ (MPa)	Ec (MPa)	n	k	$k_{,\ suggest}$
Mean	15.06	0.002	7530	11,280	3.01	0.91	1

3.3.2. Compressive and Single Compressive Stress–Strain Curves after Repeated Loading

The compression data and the Popovics curve after repeated loading represent the single compression curve and are plotted in Figure 11. The findings indicate that the data after 10,000 cycles and 50,000 cycles only slightly exceed the recommended single compression curve. Therefore, in subsequent design considerations, the single compression result can be directly employed as the design value. Since there is minimal disparity in compressive behavior after both single and repeated loading, this approach is considered more conservative.

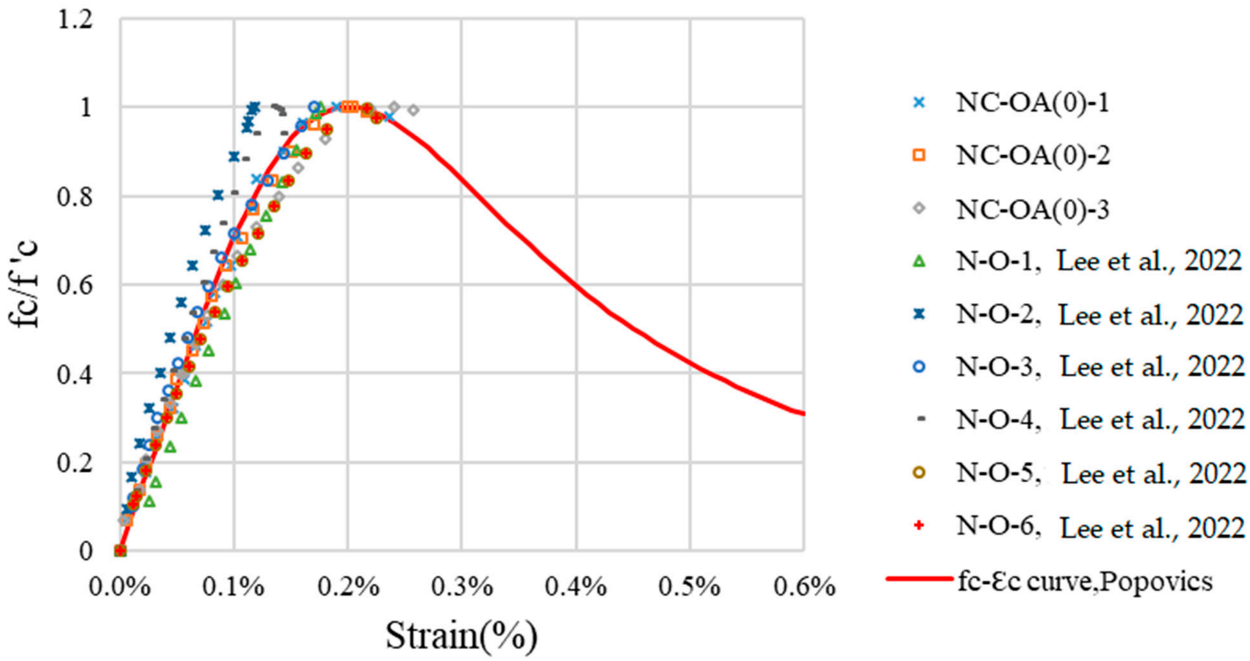

Figure 10. Comparison of Popovics stress–strain curves with experimental values.

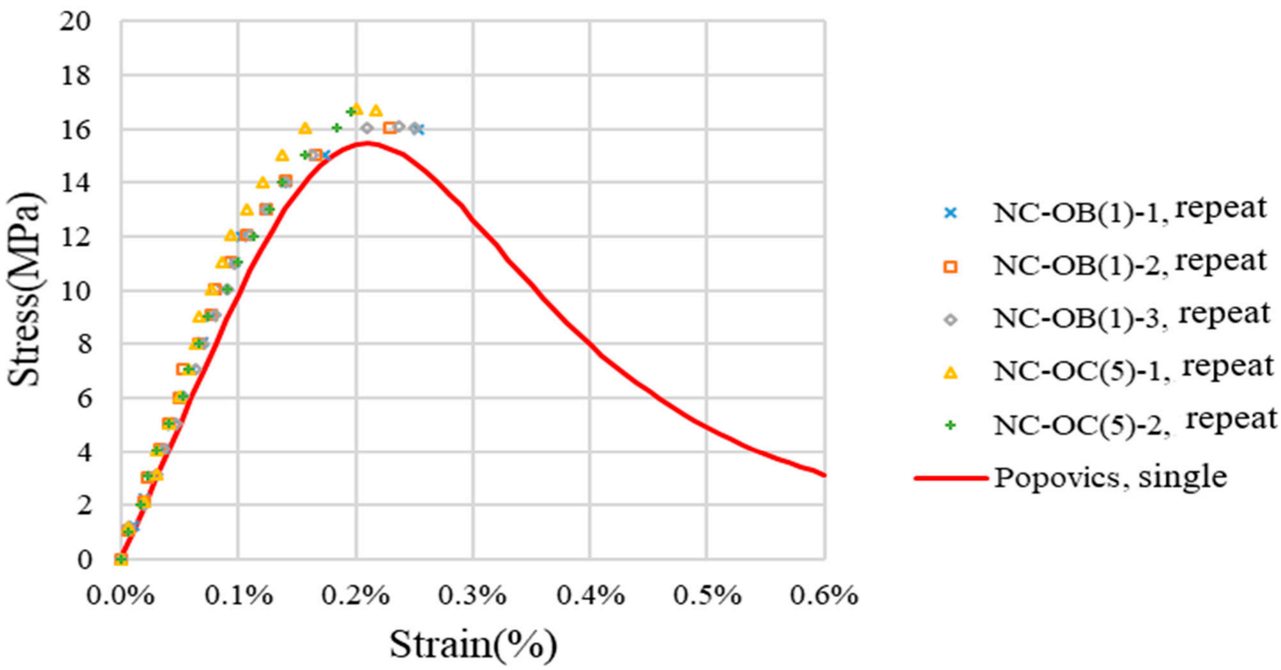

Figure 11. Comparison of Popovics stress–strain curves after single compression and repeated loading.

3.4. Results of Mechanical Behavior of Beams under Repeated Loading and Single Loading

3.4.1. Beam Bending Strength

Generally, pervious concrete has almost no steel bars or wire mesh. Without the tensile force provided by steel bars, the bottom of the pervious concrete is less able to withstand the tensile force required for cracking. In order to improve this phenomenon, glass fiber mesh and steel wire mesh were added to pervious concrete to explore the improvement effect of flexural strength after adding the fiber mesh. The bending test specimen was a reduced size beam of $100^b \times 80^h \times 500^L$ mm. Figure 12 shows the flexural strength of pervious concrete beam specimens with and without the glass fiber mesh and steel wire mesh. In the figure, the beam specimens are numbered 1 and 2, such as NB-O1 or NB-O2, which are direct single-load failure tests. Each number has two beam specimens. The specimens numbered 3 and 4, such as NB-O3 or NB-O4, are subjected to single-load failure after 50,000 cycles of repeated loading. Among them, NB-O3 and NB-O4 were damaged during 35,000 and 42,500 repeated loads, respectively, so their single compression strength after repeated loading cannot be measured. The results showed that the glass fiber mesh had no significant effect on the bending strength, but the steel mesh had a double increase in the flexural strength. The flexural rupture strength test of pervious concrete beams includes specimens with and without wire mesh and fiber-free pervious concrete by Lee et al. [7]. A total of 13 specimens were used to analyze the cracking moment coefficient. The results are shown in Table 7. It can be obtained that the average cracking coefficient of permeable concrete is 0.86. Equation (6) will be used as the subsequent design calculation of the cracking modulus (f_r) of pervious concrete.

$$fr = 0.86\sqrt{f_c{}'} \quad (6)$$

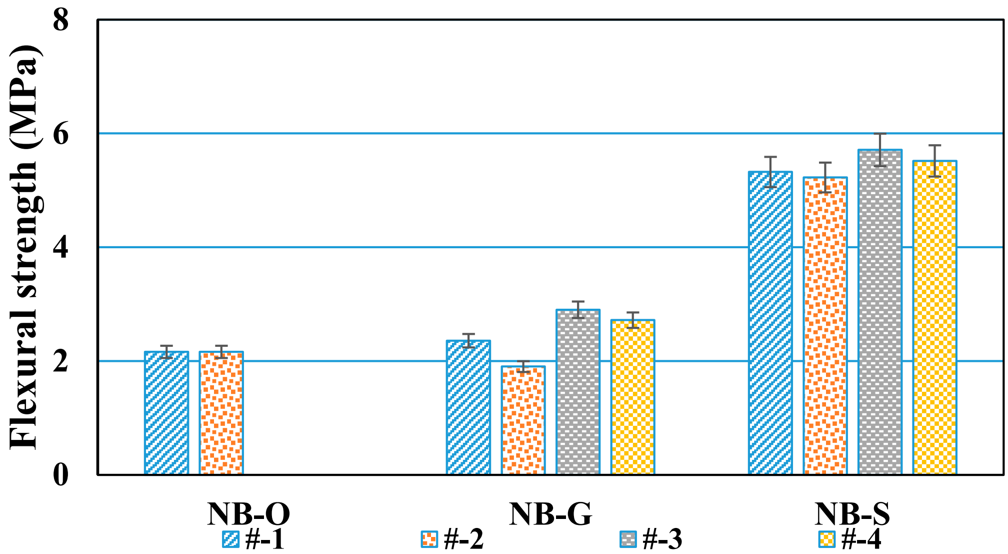

Figure 12. Flexural strength of pervious concrete beam with and without glass fiber mesh and steel mesh.

Table 7. Flexural rupture strength of pervious concrete beam specimens.

Specimen#	f_r	$f_c{}'$	$\sqrt{f_c{}'}$	k
NB-O1	2.16	15.44	3.93	0.55
NB-O2	2.16	15.44	3.93	0.55
NB-G1	2.36	15.44	3.93	0.60
NB-G2	1.90	15.44	3.93	0.48
NB-G3	2.90	15.44	3.93	0.74
NB-G4	2.72	15.44	3.93	0.69
NB-S1	5.32	15.44	3.93	1.35
NB-S2	5.23	15.44	3.93	1.33
NB-S3	5.71	15.44	3.93	1.45
NB-S4	5.52	15.44	3.93	1.40
N-O-1 [7]	3.01	14.88	3.86	0.78
N-O-2 [7]	3.33	15.19	3.90	0.85
N-O-3 [7]	2.71	15.35	3.92	0.69
Mean	3.47	15.37	3.92	0.86

3.4.2. Force Behavior of Beams during Repeated Loading

The repeated-load planning of the beam specimen in this study is 50,000 cycles, as outlined in Section 2.2.6. Some specimens without wire mesh were damaged prematurely before 50,000 cycles, so the single compression strength after repeated loading cannot be measured. During the repeated loading process, record the total displacement and the tensile and compressive strains of concrete at the initial and every 10,000 repeated loads to facilitate observation of the changes in stiffness (K) and section rigidity (E_cI_e) at each repeated stage.

The test results for stiffness and section rigidity of beam specimens, both with and without the wire mesh, during repeated loading cycles are graphically presented in Figure 13 and summarized in Table 8. It can be found that before repeated loading, the stiffness (K) of NB-O (without wire mesh) is less than that of NB-G and NB-S (with wire mesh). However, as the number of repeated loading cycles increases, the K value gradually decreases. After 10,000 cycles, the K values of the three become comparable. Additionally, the changes in section rigidity E_cI_e values for each repeated cycle show a substantial decrease at 10,000 cycles, followed by a relatively stable pattern.

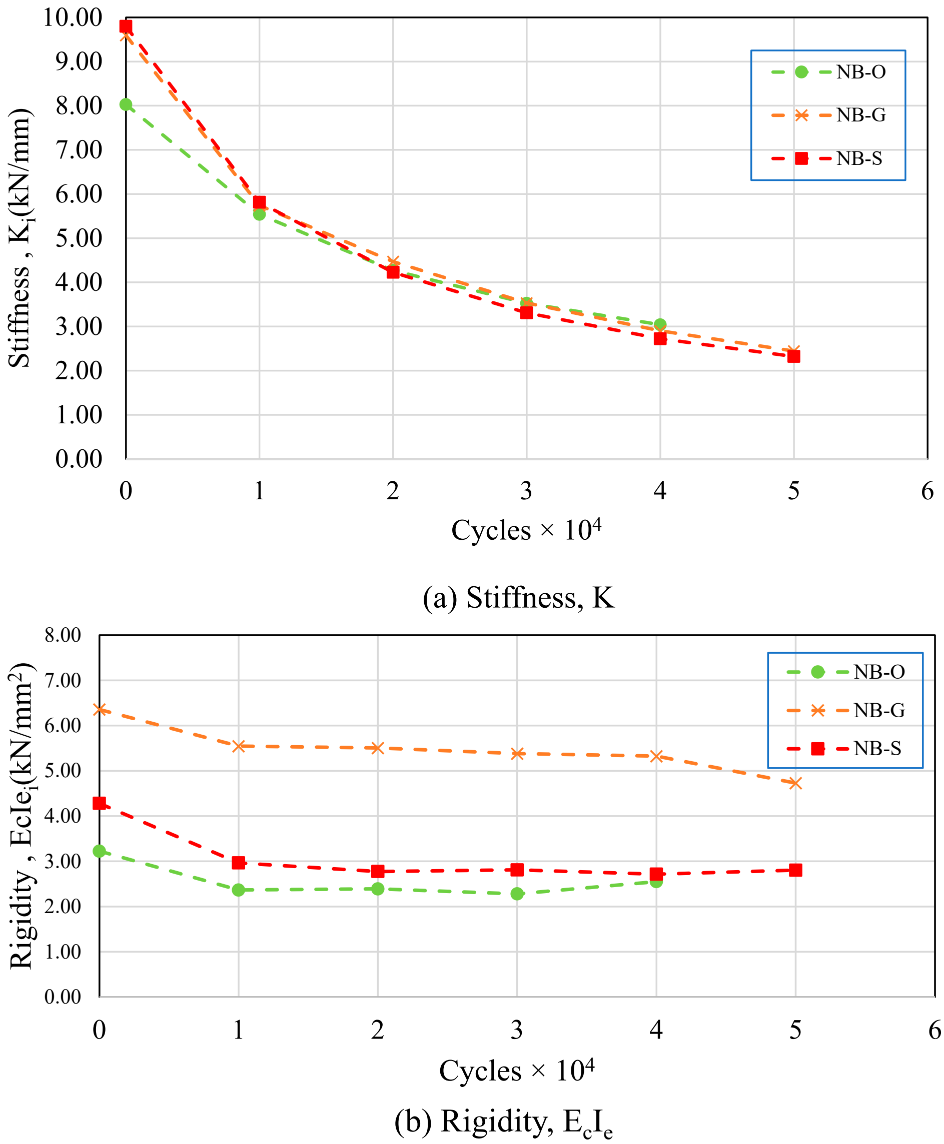

Figure 13. Changes in (**a**) stiffness and (**b**) section rigidity of beam specimens with and without wire mesh during repeated loading cycles.

Table 8. Summary table of stiffness and section rigidity of all beam specimens.

Specimen#	Cycles	(a) P (kN)	(b) Δ_i (mm)	(c) = (a)/(b) K_i (kN/mm)	$E_cI_{e,i}$ kN-mm^2 $\times 10^7$	$\frac{E_cI_{e,i}}{E_cI_{e,1}}$
NB-O (no wire mesh)	1	1.5	0.1869	8.03	3.23	1.00
	10,000	1.5	0.2708	5.54	2.37	0.73
	20,000	1.5	0.3513	4.27	2.39	0.74
	30,000	1.5	0.4253	3.53	2.28	0.71
	40,000	1.5	0.4933	3.04	2.55	0.79
	50,000	-	-	-	-	-
NB-G (glass fiber mesh)	1	1.5	0.1564	9.59	6.36	1.00
	10,000	1.5	0.2613	5.74	5.55	0.87
	20,000	1.5	0.3356	4.47	5.51	0.87
	30,000	1.5	0.4247	3.53	5.38	0.85
	40,000	1.5	0.5169	2.90	5.33	0.84
	50,000	1.5	0.6137	2.44	4.73	0.74
NB-S (steel mesh)	1	1.8	0.1837	9.80	4.28	1.00
	10,000	1.8	0.3097	5.81	2.97	0.69
	20,000	1.8	0.4259	4.23	2.78	0.65
	30,000	1.8	0.5440	3.31	2.81	0.66
	40,000	1.8	0.6611	2.72	2.72	0.63
	50,000	1.8	0.7753	2.32	2.81	0.66

Table 8 reveals that NB-O (without wire mesh) experienced failure after 40,000 repeated loads. Consequently, there are no available data on stiffness and section rigidity after 50,000 repeated loading cycles. Nonetheless, observations indicate that NB-G and NB-S (glass fiber mesh or wire mesh) initially exhibited greater stiffness and cross-sectional stiffness. However, with an increasing number of repeated loading cycles, deflection rose, leading to a subsequent reduction in stiffness. This behavior underscores the impact of repeated loading on the structural integrity and performance of pervious concrete specimens reinforced with glass fiber mesh or wire mesh.

Subsequent to the 50,000 repeated loads, single-pressure failure tests were conducted to compare the differences between failure under a single load and failure after repeated loading. The results, illustrated in Figure 14, demonstrate that the flexural strength of pervious concrete with added glass fiber mesh only experiences a slight increase, primarily enhancing ductility. This marginal improvement may be attributed to the low fiber content of the glass fiber mesh used, limiting its effectiveness in enhancing flexural strength. On the other hand, pervious concrete with added steel wire mesh exhibits a substantial increase in flexural strength, approximately doubling that of ordinary pervious concrete, accompanied by a significant improvement in ductility.

Both the glass fiber mesh and steel wire mesh specimens were subjected to single-pressure failure after 50,000 cycles of repeated loading. The load–displacement curves of the glass fiber mesh and steel wire mesh show only slight improvements. Therefore, designing based on the failure strength of a single load without considering repeated use yields conservative results. Additionally, the area enclosed by the load and displacement curves provides a measure for calculating the increased toughness and strength of pervious concrete beams due to the addition of wire mesh. The observed increase in toughness and strength aligns with findings in the existing literature on this topic [7,41].

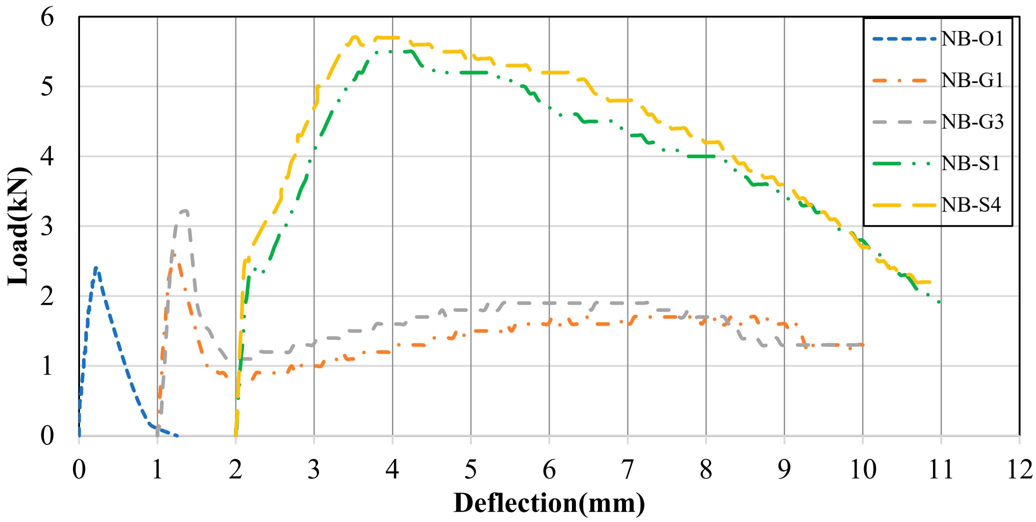

Figure 14. Comparison of repeated load–displacement diagrams of beam specimens with and without wire mesh (NB-O, NB-G and NB-S).

4. Conclusions

In summary, this study focused on pervious concrete, examining its performance with different reinforcements, elastic modulus, stress–strain curves, and various loading tests on beam specimens. The key findings and recommendations are as follows:

1. Variations in the compressive strength and elastic modulus were observed between single and repeated loading conditions. Repeated loading led to a slight increase in both compressive strength (8%) and elastic modulus (16%) due to a compaction effect.
2. The compressive strength (fc') was determined to be around 15 MPa. Empirical formulas for elastic modulus and cracking modulus, as derived in Equations (4) and (6), are useful for pervious concrete component design.
3. This study applied the Popovics stress–strain curve theory, finding that the compressive behavior aligns with typical pervious concrete behavior (Equation (5)).
4. Popovics stress–strain curves after single compression and repeated loading exhibited similar trends (correspondence only reaching strain values of 0.25%), with data after 10,000 and 50,000 loading cycles slightly exceeding the recommended single compression curve.
5. Pervious concrete initially displayed greater stiffness and section rigidity in single loading but showed a reduction in stiffness and section rigidity with an increased number of repeated loading cycles.
6. The addition of steel wire mesh to pervious concrete significantly improved flexural strength, approximately doubling that of ordinary pervious concrete, and enhanced ductility in the reinforced specimens.

Author Contributions: Conceptualization, Y.-C.W.; Methodology, W.-C.W.; Investigation, Y.-C.W. and H.-J.C.; Writing—original draft, H.-J.C.; Writing—review & editing, M.-G.L.; Visualization, L.-C.C. All authors have read and agreed to the published version of the manuscript.

Funding: The authors acknowledge the financial support provided by the Ministry of Science and Technology of Taiwan, grant number [111-2121-M-324-003].

Data Availability Statement: Data are contained within the article.

Conflicts of Interest: The authors declare no conflict of interest.

References

1. Asaeda, T.; Ca, V.T. Characteristics of Permeable Pavement during Hot Summer Weather and Impact on the Thermal Environment. *Build. Environ.* **2000**, *35*, 363–375. [CrossRef]
2. Zhong, R.; Wille, K. Compression Response of Normal and High Strength Pervious Concrete. *Constr. Build. Mater.* **2016**, *109*, 177–187. [CrossRef]
3. Bhutta, M.A.R.; Tsuruta, K.; Mirza, J. Evaluation of High-Performance Porous Concrete Properties. *Constr. Build. Mater.* **2012**, *31*, 67–73. [CrossRef]
4. Kevern, J.T. Operation, and Maintenance of Pervious Concrete Pavements. In Proceedings of the 90th Annual Meeting of the Transportation Research Board, Washington, DC, USA, 23–27 January 2011.
5. Ahmad, O.A.; Awwad, M. Effects of Polypropylene Fibers Additions on Compressive and Tensile Strengths of Concrete. *Int. J. Civ. Environ. Eng.* **2015**, *37*, 1365–1372.
6. Meng, X.; Chi, Y.; Jiang, Q.; Liu, R.; Wu, K.; Li, S. Experimental Investigation on the Flexural Behavior of Pervious Concrete Beams Reinforced with Geogrids. *Constr. Build. Mater.* **2019**, *215*, 275–284. [CrossRef]
7. Lee, M.-G.; Wang, W.-C.; Wang, Y.-C.; Lin, Y.-C.; Hsieh, Y.-C. Mechanical Properties of High Strength Pervious Concrete with Steel Fiber or Glass Fiber. *Buildings* **2022**, *12*, 620. [CrossRef]
8. Collins, M.P.; Mitchell, D. *Prestressed Concrete Structures*; Prentice-Hall: New Jersey, NJ, USA, 1991.
9. Moehle, J. *Seismic Design of Reinforced Concrete Buildings*; McGraw-Hill Education: New York, NY, USA, 2015.
10. Whitney, C.S. Design of Reinforced Concrete Members Under Flexure or Combined Flexure and Direct Compression. *ACI J. Proc.* **1937**, *33*, 483–498.
11. Popovics, S. A Review of Stress-Strain Relationships for Concrete. *ACI J.* **1970**, *67*, 243–248.
12. Rangelov, M.; Nassiri, S.; Haselbach, L.; Englund, K. Using carbon fiber composites for reinforcing pervious concrete. *Constr. Build. Mater.* **2016**, *126*, 875–885. [CrossRef]
13. Oni, B.; Xia, J.; Liu, M. Mechanical properties of pressure moulded fiber reinforced pervious concrete pavement brick. *Case Stud. Constr. Mater.* **2020**, *13*, e00431.
14. Tang, C.-W.; Cheng, C.-K.; Ean, L.-W. Mix design and engineering properties of fiber-reinforced pervious concrete using lightweight aggregates. *Appl. Sci.* **2022**, *12*, 524. [CrossRef]
15. Akand, L.; Yang, M.; Wang, X. Effectiveness of chemical treatment on polypropylene fibers as reinforcement in pervious concrete. *Constr. Build. Mater.* **2018**, *163*, 32–39. [CrossRef]
16. Khodaii, A.; Fallah, S.; Nejad, F.M. Effects of geosynthetics on reduction of reflection cracking in asphalt overlays. *Geotext. Geomembr.* **2009**, *27*, 1–8. [CrossRef]
17. Itani, H.; Saad, G.; Chehab, G. The use of geogrid reinforcement for enhancing the performance of concrete overlays: An experimental and numerical assessment. *Constr. Build. Mater.* **2016**, *124*, 826–837. [CrossRef]
18. Ferrotti, G.; Canestrari, F.; Pasquini, E.; Virgili, A. Experimental evaluation of the influence of surface coating on fiberglass geogrid performance in asphalt pavements. *Geotext. Geomembr.* **2012**, *34*, 11–18. [CrossRef]
19. Ferrotti, G.; Canestrari, F.; Virgili, A.; Grilli, A. A strategic laboratory approach for the performance investigation of geogrids in flexible pavements. *Constr. Build. Mater.* **2011**, *25*, 2343–2348. [CrossRef]
20. Sangthongtong, A.; Semvimol, N.; Rungratanaubon, T.; Duangmal, K.; Joyklad, P. Mechanical Properties of Pervious Recycled Aggregate Concrete Reinforced with Sackcloth Fibers (SF). *Infrastructures* **2023**, *8*, 38. [CrossRef]
21. Sakib, N.; Bhasin, A.; Islam, M.K.; Khan, K.; Khan, M.I. A review of the evolution of technologies to use sulphur as a pavement construction material. *Int. J. Pavement Eng.* **2021**, *22*, 392–403. [CrossRef]
22. Amin, M.N.; Iqtidar, A.; Khan, K.; Javed, M.F.; Shalabi, F.I.; Qadir, M.G. Comparison of machine learning approaches with traditional methods for predicting the compressive strength of rice husk ash concrete. *Crystals* **2021**, *11*, 779. [CrossRef]
23. Khan, K.; Ahmad, W.; Amin, M.N.; Aslam, F.; Ahmad, A.; Al-Faiad, M.A. Comparison of Prediction Models Based on Machine Learning for the Compressive Strength Estimation of Recycled Aggregate Concrete. *Materials* **2022**, *15*, 3430. [CrossRef]
24. Karalar, M.; Özkılıç, Y.O.; Deifalla, A.F.; Aksoylu, C.; Arslan, M.H.; Ahmad, M.; Sabri, M.M.S. Improvement in bending performance of reinforced concrete beams produced with waste lathe scraps. *Sustainability* **2022**, *14*, 12660. [CrossRef]
25. Çelik, A.I.; Özkılıç, Y.O.; Zeybek, Ö.; Özdöner, N.; Tayeh, B.A. Performance assessment of fiber-reinforced concrete produced with waste lathe fibers. *Sustainability* **2022**, *14*, 11817. [CrossRef]
26. Shcherban, E.M.; Stel'Makh, S.A.; Beskopylny, A.N.; Mailyan, L.R.; Meskhi, B.; Shilov, A.A.; Chernil'Nik, A.; Özkılıç, Y.O.; Aksoylu, C. Normal-Weight Concrete with Improved Stress–Strain Characteristics Reinforced with Dispersed Coconut Fibers. *Appl. Sci.* **2022**, *12*, 11734. [CrossRef]
27. Zeybek, Ö.; Özkılıç, Y.O.; Çelik, A.I.; Deifalla, A.F.; Ahmad, M.; Sabri, M.M. Performance evaluation of fiber-reinforced concrete produced with steel fibers extracted from waste tire. *Front. Mater.* **2022**, *9*, 1057128. [CrossRef]
28. Beskopylny, A.N.; Shcherban, E.M.; Stel'makh, S.A.; Meskhi, B.; Shilov, A.A.; Varavka, V.; Evtushenko, A.; Özkılıç, Y.O.; Aksoylu, C.; Karalar, M. Composition Component Influence on Concrete Properties with the Additive of Rubber Tree Seed Shells. *Appl. Sci.* **2022**, *12*, 11744. [CrossRef]
29. Revilla-Cuesta, V.; Evangelista, L.; de Brito, J.; Skaf, M.; Manso, J.M. Shrinkage prediction of recycled aggregate structural concrete with alternative binders through partial correction coefficients. *Cem. Concr. Compos.* **2022**, *129*, 104506. [CrossRef]

30. Liang, C.; You, J.; Gu, F.; Gao, Y.; Yang, G.; He, Z.; Hou, S.; Duan, S. Enhancing the elastic modulus of concrete prepared with recycled coarse aggregates of different quality by chemical modifications. *Constr. Build. Mater.* **2022**, *360*, 129590. [CrossRef]
31. Duan, Z.; Lv, Z.; Xiao, J.; Liu, C.; Nong, X. Study on the Performance of Recycled Coarse and Fine Aggregates as Microbial Carriers Applied to Self-Healing Concrete. *Materials* **2023**, *16*, 2371. [CrossRef]
32. Hussain, H.K.; Abbas, A.M.; Ojaimi, M.F. Fiber-Type Influence on the Flexural Behavior of RC Two-Way Slabs with an Opening. *Buildings* **2022**, *12*, 279. [CrossRef]
33. Tang, B.; Fan, M.; Yang, Z.; Sun, Y.; Yuan, L. A comparison study of aggregate carbonation and concrete carbonation for the enhancement of recycled aggregate pervious concrete. *Constr. Build. Mater.* **2023**, *371*, 130797. [CrossRef]
34. Bagherzadeh, F.; Shafighfard, T. Ensemble Machine Learning approach for evaluating the material characterization of carbon nanotube-reinforced cementitious composites. *Case Stud. Constr. Mater.* **2022**, *17*, e01537. [CrossRef]
35. *ASTM C39/C39M-16*; Standard Test Method for Compressive Strength of Cylindrical Concrete Specimens. ASTM International: West Conshohocken, PA, USA, 2016; pp. 1–8.
36. *ASTM C78/C78M-18*; Standard Test Method for Flexural Strength of Concrete (Using Simple Beam with Third-Point Loading). ASTM International: West Conshohocken, PA, USA, 2018; pp. 1–5.
37. *ASTM C469/C469M-22*; Standard Test Method for Static Modulus of Elasticity and Poisson's Ratio of Concrete in Compression. ASTM International: West Conshohocken, PA, USA, 2022; pp. 1–6.
38. *ACI 522R-10*; Pervious Concrete. American Concrete Institute: Farmington Hills, MI, USA, 2010; pp. 1–5.
39. Kia, A.; Wong, H.S.; Cheeseman, C.R. High-strength clogging resistant permeable pavement. *Int. J. Pavement Eng.* **2021**, *22*, 271–282. [CrossRef]
40. Hatanaka, S.; Okamoto, T.; Kajio, S.; Kunieda, M.; Mishima, N.; Hiraiwa, T. Technical Committee Report on Establishment of Construction Standards and Quality Assurance System for Performance-Based Design of Porous Concrete. *JCI* **2015**, *343*. (In Japanese)
41. Avanaki, M.J.; Abedi, M.; Hoseini, A.; Maerefat, M.S. Effects of fiber volume fraction and aspect ratio on mechanical properties of hybrid steel fiber reinforced concrete. *J. New Approaches Civ. Eng.* **2018**, *2*, 49–64.

Disclaimer/Publisher's Note: The statements, opinions and data contained in all publications are solely those of the individual author(s) and contributor(s) and not of MDPI and/or the editor(s). MDPI and/or the editor(s) disclaim responsibility for any injury to people or property resulting from any ideas, methods, instructions or products referred to in the content.